

Mock LISA Data Challenge 1: \mathcal{F} -statistic Search

Technical note

R. Prix and J. T. Whelan

December 3, 2006

Contents

| | | |
|----------|---|-----------|
| 1 | Method used | 1 |
| 1.1 | Multi-detector \mathcal{F} -statistic | 2 |
| 1.2 | Parameter-estimation | 4 |
| 1.2.1 | MLDC conventions for amplitude parameters | 6 |
| 1.3 | TDI and long-wavelength approximation | 6 |
| 1.3.1 | Doppler variables | 7 |
| 1.3.2 | Phase variables | 8 |
| 1.4 | Wide-parameter search grid | 8 |
| 1.5 | Pipeline | 10 |
| 1.5.1 | Generation of SFTs | 11 |
| 2 | Challenge Searches and Results | 11 |
| 2.1 | Challenge 1.1.1 | 11 |
| 2.2 | Challenge 1.1.2 | 11 |
| 2.3 | Challenge 1.1.3 | 11 |
| 2.4 | Challenge-1.1.4 | 12 |
| 2.5 | Challenge-1.1.5 | 12 |

1 Method used

We use the so-called \mathcal{F} -statistic, a coherent matched-filtering detection statistic first introduced by Jaranowski et al. [5] in the context of the search for continuous-wave signals in ground based detectors. This method has been implemented by the LIGO Scientific collaboration in LAL/LALApps [7], and

is currently used in the search for quasi-periodic GW signals from spinning neutron stars [e.g. see 1]. The generalization of the \mathcal{F} -statistic to a coherent multi-detector search was first obtained by Cutler and Schutz [3]. The application of the \mathcal{F} -statistic to the search of continuous-wave sources (such as galactic white-dwarf binaries) using LISA was first discussed in Królak et al. [6].

The multi-detector \mathcal{F} -statistic has been implemented in LALapps, in the code `ComputeFStatistic_v2`, which we are using for the present analysis.

1.1 Multi-detector \mathcal{F} -statistic

Here we give a brief introduction into the formalism and notation of the \mathcal{F} -statistic, see [8] for more details. As shown in [5], the dimensionless strain signal $s^X(t)$ of a continuous gravitational wave at detector X can be represented in the form

$$s^X(t) = \sum_{\mu=1}^4 \mathcal{A}^\mu h_\mu^X(t), \quad (1.1.1)$$

in terms of four signal-amplitudes \mathcal{A}^μ , which are independent of the detector X, and the detector-dependent basis waveforms $h_\mu^X(t)$. The four amplitudes \mathcal{A}^μ can be expressed in terms of two polarization amplitudes A_+ , A_\times , the initial phase ϕ_0 in the solar-system barycenter (SSB) at a reference time τ_{ref} , and the polarization angle ψ of the wave frame with respect to the equatorial coordinate system, namely

$$\mathcal{A}^1 = A_+ \cos \phi_0 \cos 2\psi - A_\times \sin \phi_0 \sin 2\psi, \quad (1.1.2a)$$

$$\mathcal{A}^2 = A_+ \cos \phi_0 \sin 2\psi + A_\times \sin \phi_0 \cos 2\psi, \quad (1.1.2b)$$

$$\mathcal{A}^3 = -A_+ \sin \phi_0 \cos 2\psi - A_\times \cos \phi_0 \sin 2\psi, \quad (1.1.2c)$$

$$\mathcal{A}^4 = -A_+ \sin \phi_0 \sin 2\psi + A_\times \cos \phi_0 \cos 2\psi. \quad (1.1.2d)$$

We can further relate the two polarization amplitudes A_+ and A_\times to the overall amplitude h_0 and the inclination angle ι of the quadrupole rotation axis with respect to the line of sight, namely

$$A_+ = \frac{1}{2} h_0 (1 + \cos^2 \iota), \quad A_\times = h_0 \cos \iota. \quad (1.1.3)$$

The four basis waveforms $h_\mu^X(t)$ can be written as

$$\begin{aligned} h_1^X(t) &= a^X(t) \cos \phi^X(t), & h_2^X(t) &= b^X(t) \cos \phi^X(t), \\ h_3^X(t) &= a^X(t) \sin \phi^X(t), & h_4^X(t) &= b^X(t) \sin \phi^X(t), \end{aligned} \quad (1.1.4)$$

where $a^X(t)$ and $b^X(t)$ are the antenna-pattern functions (see Eqs.(12,13) of [5]), and $\phi^X(t)$ is the signal phase at the detector X. The antenna-pattern functions $a^X(t)$, $b^X(t)$ depend on the sky position of the GW source (which is equivalent to the propagation direction \hat{k} of the wave), and on the location and orientation of the detector X. The phase $\phi^X(t)$ also depends on the *intrinsic* phase parameters, ω say, of the signal. In the case of continuous waves from isolated neutron stars, ω would only consist of the $s + 1$ spin parameters, i.e. $\omega = \{f^{(k)}\}_{k=0}^s$, where $f^{(k)}$ is the k -th time-derivative of the intrinsic signal frequency in the SSB.

In the following we denote the set of ‘‘Doppler parameters’’ (i.e. the parameters affecting the time evolution of the phase) by $\lambda \equiv \{\hat{k}, \omega\}$, as opposed to the four ‘‘amplitude parameters’’ $\{\mathcal{A}\}^\mu = \mathcal{A}^\mu$.

Using the multi-detector notation of [3, 6], we write vectors in ‘‘detector-space’’ in boldface, i.e. $\{\mathbf{s}\}^X = s^X$, and so the signal model (1.1.1) can be written as

$$\mathbf{s}(t; \mathcal{A}, \lambda) = \mathcal{A}^\mu \mathbf{h}_\mu(t; \lambda), \quad (1.1.5)$$

with implicit summation over repeated amplitude indices, $\mu \in \{1, 2, 3, 4\}$.

The multi-detector scalar product is defined as

$$(\mathbf{x}|\mathbf{y}) \equiv \int_{-\infty}^{\infty} \tilde{x}^X(f) S_{XY}^{-1}(f) \tilde{y}^{Y*}(f) df, \quad (1.1.6)$$

where $\tilde{x}(f)$ denotes the Fourier transform of $x(t)$. We use implicit summation over repeated detector indices, and the inverse noise matrix is defined by $S_{XY}^{-1} S^{YZ} = \delta_X^Z$. In the case of uncorrelated noise, where $S^{XY} = S^X \delta^{XY}$, the scalar product simplifies to

$$(\mathbf{x}|\mathbf{y}) = \sum_X (x^X|y^X), \quad (1.1.7)$$

in terms of the usual single-detector scalar product

$$(x^X|y^X) \equiv \int_{-\infty}^{\infty} \frac{\tilde{x}^X(f) \tilde{y}^{X*}(f)}{S^X(f)} df. \quad (1.1.8)$$

With the signal model (1.1.1), the log-likelihood ratio is found as

$$\ln \Lambda(\mathbf{x}; \mathcal{A}, \lambda) = \mathcal{A}^\mu x_\mu - \frac{1}{2} \mathcal{A}^\mu \mathcal{M}_{\mu\nu} \mathcal{A}^\nu, \quad (1.1.9)$$

where we defined

$$x_\mu(\lambda) \equiv (\mathbf{x}|\mathbf{h}_\mu), \quad (1.1.10)$$

$$\mathcal{M}_{\mu\nu}(\lambda) \equiv (\mathbf{h}_\mu|\mathbf{h}_\nu). \quad (1.1.11)$$

We see that the likelihood ratio (1.1.9) can be maximized analytically with respect to the unknown amplitudes \mathcal{A}^μ , resulting in the maximum-likelihood estimators

$$\mathcal{A}_{\text{MLE}}^\mu = \mathcal{M}^{\mu\nu} x_\nu. \quad (1.1.12)$$

Substituting this into the detection statistic, we obtain the so-called \mathcal{F} -statistic, namely

$$2\mathcal{F}(\mathbf{x}; \lambda) \equiv x_\mu \mathcal{M}^{\mu\nu} x_\nu, \quad (1.1.13)$$

where $\mathcal{M}^{\mu\nu} \equiv \{\mathcal{M}^{-1}\}^{\mu\nu}$, i.e. $\mathcal{M}_{\mu\alpha} \mathcal{M}^{\alpha\nu} = \delta_\mu^\nu$.

Let us consider the case where the target Doppler parameters λ are perfectly matched to the signal λ_s , we find the expectation value of the \mathcal{F} -statistic as

$$E[2\mathcal{F}] = 4 + \text{SNR}^2, \quad (1.1.14)$$

in terms of the ‘‘optimal’’ signal-to-noise ratio SNR, which is expressible as

$$\text{SNR}^2 = s_\mu \mathcal{M}^{\mu\nu} s_\nu = \mathcal{A}^\mu \mathcal{M}_{\mu\nu} \mathcal{A}^\nu = (\mathbf{s}|\mathbf{s}). \quad (1.1.15)$$

1.2 Parameter-estimation

From the expression (1.1.12) for the maximum-likelihood amplitudes \mathcal{A}^μ in terms of the measured F_a, F_b , we can infer the signal-parameters A_+, A_\times (or equivalently $h_0, \cos \iota$) and ψ, ϕ_0 , by using (1.1.3) and (1.1.2). We compute the two quantities

$$A_s^2 \equiv \sum_{\mu=1}^4 (\mathcal{A}^\mu)^2 = A_+^2 + A_\times^2, \quad (1.2.1)$$

$$D_a \equiv \mathcal{A}^1 \mathcal{A}^4 - \mathcal{A}^2 \mathcal{A}^3 = A_+ A_\times, \quad (1.2.2)$$

which can easily be solved for A_+, A_\times , namely

$$2A_{+, \times}^2 = A_s^2 \pm \sqrt{A_s^4 - 4D_a^2}, \quad (1.2.3)$$

where our convention here is $|A_+| \geq |A_\times|$, cf. (1.1.3), and therefore the ‘+’ solution is A_+ , and the ‘-’ is A_\times . The sign of A_+ is always positive by this convention, while the sign of A_\times is given by the sign of D_a , as can be seen from (1.2.2). Note that the discriminant in (1.2.3) is also expressible as

$$\text{disc} \equiv \sqrt{A_s^4 - 4D_a^2} = A_+^2 - A_\times^2 \geq 0. \quad (1.2.4)$$

Having computed A_+, A_\times , we can now also obtain ψ and ϕ_0 , namely defining $\beta \equiv A_\times/A_+$, and

$$b_1 \equiv \mathcal{A}^4 - \beta \mathcal{A}^1, \quad (1.2.5)$$

$$b_2 \equiv \mathcal{A}^3 + \beta \mathcal{A}^2, \quad (1.2.6)$$

$$b_3 \equiv \beta \mathcal{A}^4 - \mathcal{A}^1, \quad (1.2.7)$$

we easily find

$$\psi = \frac{1}{2} \operatorname{atan} \left(\frac{b_1}{b_2} \right). \quad (1.2.8)$$

and

$$\phi_0 = \operatorname{atan} \left(\frac{b_2}{b_3} \right). \quad (1.2.9)$$

The amplitudes \mathcal{A}^μ are seen from (1.1.2) to be invariant under the following gauge-transformation, namely *simultaneously* $\{\psi \rightarrow \pi/2, \phi_0 \rightarrow \phi_0 + \pi\}$. Applying this twice, and taking account of the trivial gauge-freedom by 2π , this also contains the invariance $\psi \rightarrow \psi + \pi$. Note that there is still an overall sign-ambiguity in the amplitudes \mathcal{A}^μ , which can be determined as follows: compute a 'reconstructed' \mathcal{A}_r^μ from (1.1.2) using the estimates $A_{+, \times}$ and ψ, ϕ_0 , and compare its sign to the original estimate \mathcal{A}^μ of (1.1.12). If the sign differs, the correct solution is simply found by replacing $\phi_0 \rightarrow \phi_0 + \pi$.

In order to fix a unique gauge, we restrict the quadrant of ψ to be $\psi \in [-\pi/4, \pi/4]$ (in accord with the TDS convention), which can always be achieved by the above gauge-transformation, while ϕ_0 remains unconstrained in $\phi_0 \in [0, 2\pi)$.

Converting A_+, A_\times into h_0 and $\mu \equiv \cos \iota$ is done by solving (1.1.3), which yields

$$h_0 = A_+ + \sqrt{A_+^2 - A_\times^2}, \quad (1.2.10)$$

where we only kept the '+' solution, as we must have $h_0 > A_+$. Finally, $\mu = \cos \iota$ is simply given by $\cos \iota = A_\times / h_0$.

We know that the errors dx_μ satisfy (assuming Gaussian noise):

$$E[dx_\mu dx_\nu] = \mathcal{M}_{\mu\nu}. \quad (1.2.11)$$

As a consequence of (1.1.12), we therefore obtain the covariance-matrix of the estimation-errors $d\mathcal{A}^\mu$ as

$$E[d\mathcal{A}^\mu d\mathcal{A}^\nu] = \mathcal{M}^{\mu\nu}, \quad (1.2.12)$$

which corresponds to the Cramér-Rao bound, and $\mathcal{M}^{\mu\nu}$ is seen to be the inverse Fisher-matrix. The corresponding Fisher matrix for the variables $\{h_0, \cos \iota, \psi, \phi_0\}$ is simply obtained from the above together with the appropriate Jacobian accounting for the variables-transformation from \mathcal{A}^μ .

1.2.1 MLDC conventions for amplitude parameters

Unfortunately, the MLDC conventions for the amplitude parameters differ from the above standard LIGO/CW definitions for $\{h_0, \cos \iota, \psi, \phi_0\}$. Here we only summarize without derivation how the “translation” is performed:

- MLDC “Amplitude” = $h_0/2$
- MLDC “Inclination” = $\pi - \iota$
- MLDC “Polarization” = $\pi/2 - \psi$
- MLDC “InitialPhase” = ϕ_0 (yea!)

Note: using these translations we still observe a systematic difference of π in ϕ_0 with respect to the “InitialPhase” for the Training-sets 1.1.1abc, 1.1.2. We therefore tentatively “fixed” this phase-error (equivalent to an overall sign-change of the waveform). In Challenge 1.1.3, however, the “InitialPhase” suddenly seems to agree with ϕ_0 *without* the phase-difference of π ! This indicates either a problem in our codes, or in the production of the MLDC data-sets.

1.3 TDI and long-wavelength approximation

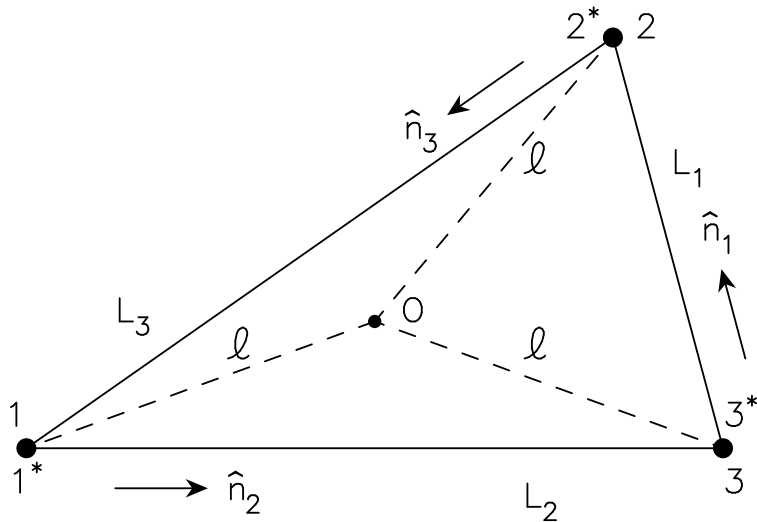


Figure 1: LISA configuration and TDI conventions used.

In the following we assume a stationary LISA array (cf. Fig. 1), and denote \vec{p}_i the vectors from the guiding center \mathcal{O} to i . We assume here and in the following that the LISA geometry is measured in light-travel time, e.g. $L \equiv \tilde{L}/c$, where \tilde{L} is measured in units of length.

1.3.1 Doppler variables

The single-arm Doppler response to a GW $y_{slr}^{\text{GW}}(t) \sim \Delta\nu/\nu$ of the light path $s \rightarrow r$ along arm l can be shown [4, 2] to be

$$y_{slr}^{\text{GW}} = (1 + \epsilon_{slr} \hat{k} \cdot \hat{n}_l) \left[\Psi_l(t - \hat{k} \cdot \vec{p}_s - L_l) - \Psi_l(t - \hat{k} \cdot \vec{p}_r) \right], \quad (1.3.1)$$

where

$$\Psi_l \equiv \frac{1}{2} \frac{\hat{n}_l \cdot \overleftrightarrow{h} \cdot \hat{n}_l}{1 - (\hat{k} \cdot \hat{n}_l)^2}. \quad (1.3.2)$$

Note the geometrical identity $\vec{p}_r - \vec{p}_s = L_l \hat{n}_l \epsilon_{slr}$. We further introduce the time-delay operator

$$y_{slr,d_1\dots d_m}(t) = y_{slr}(t - L_{d_1} - \dots - L_{d_m}). \quad (1.3.3)$$

Various TDI-observables can be constructed from the single-arm building blocks (1.3.1) with suitable time-delays (1.3.3) as to cancel the (otherwise dominating) laser-noise. One such set of 3 laser-noise free observables is X, Y, Z , defined as

$$X \equiv y_{132,322} - y_{123,233} + y_{231,22} - y_{321,33} + y_{123,2} - y_{132,3} + y_{321} - y_{231}, \quad (1.3.4)$$

and Y and Z are given by cyclic permutations of $\{1, 2, 3\}$. Geometrically these observables correspond to a 'double-arm' interferometer, e.g. for X one light-path is $1 \rightarrow 3 \rightarrow 1 \rightarrow 2 \rightarrow 1$ and the second 'arm' is $1 \rightarrow 2 \rightarrow 1 \rightarrow 3 \rightarrow 1$.

To simplify matters, we will here restrict ourselves to work in the long-wavelength limit (LWL). The characteristic timescale on which a GW of frequency f is changing is given by $\dot{h} \sim 2\pi f \mathcal{O}(h)$, so the characteristic length-scale is $\lambda/2\pi$, the so-called reduced wavelength. The LWL is therefore characterized by assuming $|\vec{p}_l| \sim L = \tilde{L}/c \ll \lambda/2\pi c$, which would be valid for GW frequencies $f \ll 1/(2\pi L) \sim 10$ mHz, assuming an arm-length of $L \sim 5 \times 10^6$ km/ $c \sim 17$ s. We can therefore Taylor-expand in $\epsilon \equiv 2\pi f L \ll 1$. The LWL of the single-arm GW responses (1.3.1) is found as

$$y_{slr}^{\text{GW}} = -\frac{L_l}{2} \hat{n}_l \cdot \overleftrightarrow{h} \cdot \hat{n}_l + \mathcal{O}(\epsilon^2). \quad (1.3.5)$$

Note that the Doppler-readouts contain no zero-order contributions in L , i.e. $y_{slr}^{\text{GW}} = \mathcal{O}(\epsilon)$.

In order to express (1.3.4) in the LWL, we also need to expand the time-delays (1.3.3), namely

$$y_{slr,d_1\dots d_m}(t) = y_{slr}(t) - \dot{y}_{slr}(t) (L_{d_1} + \dots + L_{d_m}) + \mathcal{O}(\epsilon^2). \quad (1.3.6)$$

Using this and the symmetry of the first-order term (1.3.5), we can expand X , defined in (1.3.4), in the form

$$X = 4L_3 \dot{y}_{123}^{(1)} - 4L_2 \dot{y}_{231}^{(1)} + \mathcal{O}(\varepsilon^3). \quad (1.3.7)$$

Plugging in the expansion (1.3.5) of the Doppler readouts, we find the lowest-order contribution as

$$X^{(2)} = -2L_2L_3 (\hat{n}_2 \otimes \hat{n}_2 - \hat{n}_3 \otimes \hat{n}_3) : \overset{\leftrightarrow}{\overset{\leftrightarrow}{h}}, \quad (1.3.8)$$

which corresponds to the standard LWL expression for the measured strain $h(t)$ of ground-based detectors, up to a constant pre-factor of $-4L_2L_3$ and the second time-derivative of $\overset{\leftrightarrow}{h}$, i.e. we could write $X^{(2)} = -4L_2L_3 \ddot{h}_{23}(t)$, where $h_{23}(t) \equiv \overset{\leftrightarrow}{d}_{23} : \overset{\leftrightarrow}{h}$ and where we defined the detector-tensor $\overset{\leftrightarrow}{d}_{ij}$ as

$$\overset{\leftrightarrow}{d}_{ij} \equiv \frac{1}{2} (\hat{n}_i \otimes \hat{n}_i - \hat{n}_j \otimes \hat{n}_j). \quad (1.3.9)$$

The remaining observables Y, Z are obtained by cyclic index-permutation

$$X^{(2)} = -4L_2L_3 \overset{\leftrightarrow}{d}_{23} : \overset{\leftrightarrow}{h}, \quad (1.3.10a)$$

$$Y^{(2)} = -4L_3L_1 \overset{\leftrightarrow}{d}_{31} : \overset{\leftrightarrow}{h}, \quad (1.3.10b)$$

$$Z^{(2)} = -4L_1L_2 \overset{\leftrightarrow}{d}_{12} : \overset{\leftrightarrow}{h}, \quad (1.3.10c)$$

which gives us the explicit relation (to lowest order) between the TDI-observables X, Y, Z given in the MLDC, and the GW tensor $\overset{\leftrightarrow}{h}$ as used in the \mathcal{F} -statistic analysis, as discussed in Sec. 1.1.

1.3.2 Phase variables

1.4 Wide-parameter search grid

For simplicity we used a “foliated” template grid **Freq x Sky** in the Doppler parameter space $\Delta\lambda = \{f, \alpha, \delta\}$, consisting of a *isotropic* sky-grid with step-sizes at the equator:

$$d\alpha(0) = d\delta = \frac{\sqrt{2m}}{(R_{\text{orb}}/c)2\pi f}, \quad (1.4.1)$$

while for different latitudes we’ll use $d\alpha(\delta) = d\alpha(0)/\cos(\delta)$, in order to obtain an isotropic sky-grid. The frequency step-size is given by

$$df = \frac{\sqrt{12m}}{\pi T}, \quad (1.4.2)$$

where m is the desired maximal mismatch, f is the search-frequency and T the length of observation. The expression for the frequency-resolution is the standard metric frequency stepsize, while the sky-resolution is approximately valid for observation times $T \gtrsim 1/2$ year, and can be derived from the orbital phase-metric. In Fig. 2, these grid step sizes are denoted by $dD \equiv \{df, d\alpha, d\delta\}$.

1.5 Pipeline

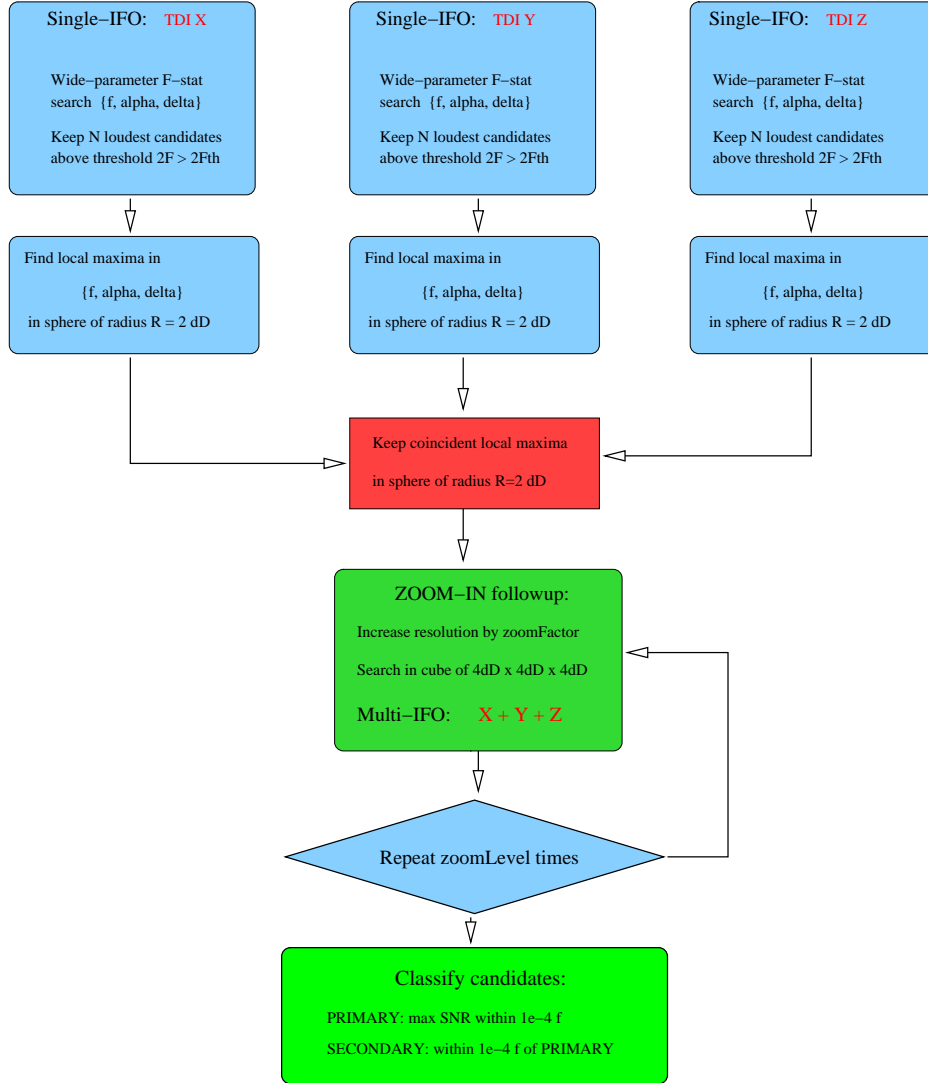


Figure 2: Schematic representation of wide-parameter pipeline. dD denotes the grid step-sizes discussed in Sec. 1.4.

For the wide-parameter searches, we use the pipeline shown in Fig. 2, where we typically keep the $N = 20,000$ loudest candidates above $SNR > 10$ in the first stage, and zoom by a factor $zoomFactor = 10$ for $zoomLevel = 2$ times in the third stage, yielding a refinement of a factor of 100 with respect to the initial wide-parameter grid. The search-grid in the first stage is constructed for a maximal mismatch of $m \sim 0.3 - 0.4$.

Several secondary maxima of true signals pass the triple-coincidence step and cannot be discarded or distinguished without further study. These secondary candidates are typically found within a frequency band of up to $\Delta f \lesssim 1.4 \times 10^{-4} f$ of the true signal frequency f . In the last step, we therefore classify all triple-coincident candidates as PRIMARY or SECONDARY: beginning with the loudest unclassified candidate, all candidates within Δf of this candidate are classified as SECONDARY. We then proceed to the next loudest candidate until all candidates have been processed. However, this algorithm will classify true signals as SECONDARY if they lie too close to each other, which happens in Challenges 1.1.4 and 1.1.5. Further study is required for a finer distinction of true signals and secondary maxima.

1.5.1 Generation of SFTs

2 Challenge Searches and Results

The primary candidates of the different searches are found in the files `RESULT_*.dat`, while the corresponding secondary candidates are given for references in the files `SECONDARY_*.dat`. Note: while the first-stage threshold is on the single-IFO SNR, the last column 'SNR' in the result files give the final multi-IFO SNR using the combined TDI channels X, Y and Z.

2.1 Challenge 1.1.1

The first-stage single-IFO threshold used as $2\mathcal{F} > 100$, corresponding to an SNR $\gtrsim 10$. A single PRIMARY candidate passed the pipeline in each of the challenges 1.1.1a, 1.1.1b and 1.1.1c.

2.2 Challenge 1.1.2

No wide-parameter search pipeline was required, as the Doppler-positions $\{f, \alpha, \delta\}$ of the sources were given: we therefore performed a single-template search for each source position and estimated its amplitude parameters $\{h_0, \cos \iota, \psi, \phi_0\}$, as described in Sec. 1.2.

2.3 Challenge 1.1.3

The specification of this challenge stated that all signals would be above SNR > 10 . However, a targeted search on the Training-set, using the Doppler-parameters given in the key, showed that `b1tOPEN113`, `b1tOPEN115` and `b1tOPEN116` had single-IFO SNRs below 10 (namely 7.5, 4.3 and 6.0

respectively). We therefore lowered the first-stage single-IFO threshold to $2\mathcal{F} > 30$ (i.e. $\text{SNR} \gtrsim 5$), and we found 16 (LISAsim) and 17 (synthLISA) primary candidates out of the injected 20 signals. The missed signals most likely have a too low SNR to be detected in the first stage despite the lower threshold, given that the discrete template grid used had a maximal mismatch of $m = 0.4$.

2.4 Challenge-1.1.4

We used a first-stage single-IFO threshold of $2\mathcal{F} > 20$ ($\text{SNR} \gtrsim 4$). The classification algorithm resulted in a total of 26 (LISAsim) and 24 (synthLISA) PRIMARY candidates respectively. Many missed signals were most likely classified as SECONDARY maxima due to the closeness in frequency of the signals.

2.5 Challenge-1.1.5

Using the same threshold of $2\mathcal{F} > 20$, we found only 5 PRIMARY candidates, both with synthLISA and LISAsim data. This is expected from the high density of signals in a very narrow frequency band and our classification algorithm using a frequency band of $\Delta f = 1.4 \times 10^{-4} f$. In fact, running the classification on the signal-parameters of the Training-set *key* yielded only 6 primary candidates. A more detailed understanding of the parameter-space structure is required to be able to distinguish secondary maxima from true signals within the Doppler window of Δf .

References

- [1] B. Abbott et al. Coherent searches for periodic gravitational waves from unknown isolated sources and Scorpius X-1: results from the second LIGO science run. *submitted*, 2006. (LIGO Scientific Collaboration) (preprint gr-qc/0605028).
- [2] J. W. Armstrong, F. B. Estabrook, and M. Tinto. Time-Delay Interferometry for Space-based Gravitational Wave Searches. *ApJ*, 527:814–826, Dec. 1999. doi: 10.1086/308110.
- [3] C. Cutler and B. F. Schutz. The generalized F-statistic: multiple detectors and multiple gravitational wave pulsars. *Phys. Rev. D.*, 72:063006, 2005.

- [4] F. B. Estabrook and H. D. Wahlquist. Response of Doppler spacecraft tracking to gravitational radiation. *GRGr*, 6:439–447, 1975.
- [5] P. Jaranowski, A. Królak, and B. F. Schutz. Data analysis of gravitational-wave signals from spinning neutron stars: The signal and its detection. *Phys. Rev. D.*, 58:063001, 1998.
- [6] A. Królak, M. Tinto, and M. Vallisneri. Optimal filtering of the lisa data. *Phys. Rev. D.*, 70:022003, 2004.
- [7] LIGO Scientific Collaboration. LAL/LALApps: FreeSoftware (GPL) tools for data-analysis. <http://www.lsc-group.phys.uwm.edu/daswg/>.
- [8] R. Prix. The search for continuous gravitational waves: metric of the multi-detector F-statistic. *accepted for publication in PRD*, 2006. (preprint gr-qc/0606088).